

Plasmonic Sensor Monolithically Integrated with a CMOS Photodiode

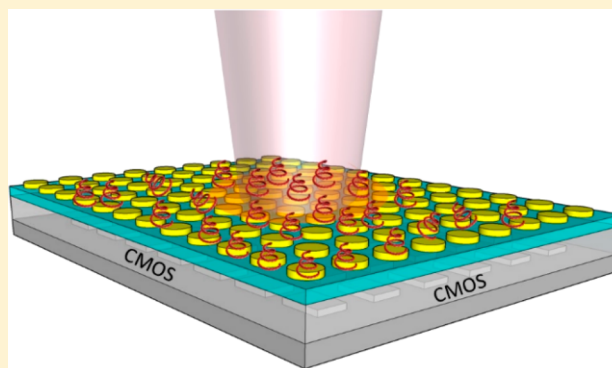
Abdul Shakoor,^{*,†} Boon C. Cheah,[†] Danni Hao,[†] Mohammed Al-Rawhani,[†] Bence Nagy,[†] James Grant,[†] Carl Dale,[‡] Neil Keegan,[‡] Calum McNeil,[‡] and David R. S. Cumming^{*,†}

[†]School of Engineering, University of Glasgow, Oakfield Avenue, Glasgow, G12 8LT, U.K.

[‡]Institute of Cellular Medicine, Newcastle University, Newcastle upon Tyne, NE2 4HH, U.K.

ABSTRACT: Complementary metal oxide semiconductor (CMOS) technology has made personal mobile computing and communications an everyday part of life. In this paper we present a nanophotonic integrated CMOS-based biosensor that will pave the way for future personalized medical diagnostics. To achieve our aim, we have monolithically integrated plasmonic nanostructures with a CMOS photodiode. Following this approach of monolithic nanophotonics–microelectronics integration, we have successfully developed a miniaturized nanophotonic sensor system with direct electrical readout, which eliminates the need of bulky and costly equipment that is presently used for interrogation of nanophotonic sensors. The optical sensitivity of the plasmonic nanostructures is measured to be 275 nm/refractive index unit (RIU), which translates to an electrical sensitivity of 5.8 V/RIU in our integrated sensor system. This advance is the first demonstration of monolithic integration of nanophotonic structures with CMOS detectors and is a crucial step toward translating laboratory based nanophotonic sensing systems to portable, low-cost, and digital formats.

KEYWORDS: plasmonic sensors, nanophotonics, CMOS, nanophotonics–microelectronics integration



Microelectronics technology has revolutionized the electronics industry and ensured its widespread applicability in a number of areas, especially computing and communications. New developments in complementary metal oxide semiconductor (CMOS) technology promises to enable new and miniaturized sensors for applications in point-of-care diagnostics and precision medicine.¹ In the same way the CMOS has revolutionized personal computing, we anticipate that it can also transform personalized medicine.² Integrating nanophotonic sensors with CMOS technology can lead to a new class of sensors by combining advantages of both technologies with applications in point-of-care diagnostics.

Developing efficient nanophotonic sensors is a very active area of research, which in addition to improving the performance in terms of sensitivity and detection limit^{3,4} is also aimed at miniaturization.⁵ The need of developing miniaturized sensor systems is ever increasing to enhance applicability and reduce cost. Nanophotonic sensors based on different material platforms have been demonstrated^{6–13} and can be broadly classified into two main groups: (1) metal based^{6–8} and (2) dielectric or semiconductor based such as silicon nitride^{9,10} or silicon.^{11–13} In addition to different material platforms, different designs such as cavity,^{11–15} waveguide,^{4,16–18} or grating^{19,20}-based devices have been demonstrated. Over the past decade remarkable progress has been made in improving the sensor performance parameters such as sensitivity. Furthermore, the inherent size of the sensor itself is on the order of only a few hundred nanometers or a few

micrometers, thus contributing to the goal of making compact sensors. However, one common drawback in these nanophotonic sensors is that their interrogation requires external bulky and costly equipment such as lasers and optical spectrum analyzers that not only increases the cost but also removes the advantage of compactness of the sensor chip and makes the widespread applicability of the sensor system impractical. To make the use of nanophotonic sensors practical in everyday life, it is important to make the complete sensor system including the interrogation system compact and portable. This can be achieved by integrating the nanophotonic sensors with detectors such as a photodiode (PD) to have a direct electrical readout. Integrating nanophotonic sensors with well established CMOS technology offers great promise in terms of compactness, lower cost for mass production, multiplexing, and ease of merging photonic and electronic functionalities. There are only a few reports on the integration of nanophotonic structures with CMOS technology to develop a compact sensing system. Nanophotonic structures have been integrated with a CMOS chip to act as a filter in fluorescence sensing.²¹ However, this work did not use the advantage of label-free sensing offered by nanophotonic sensors. Label-free sensing by utilizing nanophotonic structures and integrating them with CMOS technology has been demonstrated.²² But in this work, the

Received: June 27, 2016

Published: September 16, 2016

nanophotonic and CMOS chips are separate and positioned on top of one another, which not only increases the distance between the nanophotonic sensor and detector but also requires holders for the chip, which precludes the advantages offered by monolithic integration. Furthermore, in this work a CMOS CCD imager is used and electrical readout is not shown. In another report, a direct electrical readout is obtained, but nanophotonic sensors are integrated with a bulk silicon diode,²³ which compromises the compactness of the sensor system. In this report we have monolithically integrated nanophotonic metallic structures with CMOS PDs and demonstrated a fully packaged sensor system having a direct electrical readout. This monolithic photonic–electronic integration creates the potential for a fully portable sensing system by exploiting the information handling and processing capabilities of microelectronics on the same chip.

■ PERIODIC GOLD NANODISC ARRAY PLASMONIC SENSOR

Design. Nanophotonic sensors are often composed of resonant structures and are based on the phenomenon of refractive index sensing, where a change in the refractive index of the surrounding environment causes a shift in the resonance wavelength of the structures, which is measured by a spectrometer. The degree of wavelength shift ($\Delta\lambda$) due to the change in the refractive index measured in refractive index units (RIU) is called sensitivity (S). The sensitivity is expressed in units of nm/RIU and is considered the most important performance parameter of nanophotonic sensors.²⁴ To gauge the performance of nanophotonic sensors, a figure of merit (FOM) is often defined as a ratio of sensitivity to resonance line width ($\delta\lambda$) ($\text{FOM}_{\text{optical}} = S/\delta\lambda$). However, for PD-integrated nanophotonic sensors, it is the change in light intensity (ΔI) due to a refractive index change that is measured by a PD and converted to change in the output voltage (ΔV), which makes the effect of line width and spectral contrast even more significant. A new electrical FOM for detector-integrated nanophotonic sensors can be introduced as the ratio of change in output voltage to RIU ($\text{FOM}_{\text{electrical}} = \Delta V/\text{RIU}$). The change in intensity due to refractive index change can be improved mainly by three factors: higher sensitivity, smaller resonance line width, and larger spectral contrast. The higher the sensitivity of the resonant structures, the greater the wavelength shift for a certain RIU, leading to a larger change in intensity detected by the PD. Similarly, for a narrower resonance line width and a larger spectral contrast, the change of intensity detected by the PD for an RIU will be larger. Hence, it is important to consider all these factors while designing the nanophotonic sensors to integrate with the PD. In terms of sensitivity, nanophotonic sensors composed of metallic nanostructures show high sensitivity.^{25–27} The high sensitivity achieved by sensors made of metallic nanostructures is attributed to the phenomenon of surface plasmon resonance, which is the oscillation of conduction electrons of the metal triggered by the incident photons having the same momentum at the metal–dielectric interface. The plasmon resonance creates a high intensity electric field at the metal–dielectric interface, which causes a larger resonance shift on binding an analyte to the metal surface. However, one drawback in using plasmonic structures for integration with CMOS detectors for sensing applications is their large line width, which is caused due to inherent high losses associated with metallic structures primarily due to absorption and scattering. While a broad line

width is detrimental to achieving a large intensity change due to the wavelength shift, it has an advantage of having a large dynamic range (capability to measure big changes in refractive index before changes in intensity due to wavelength shift saturates). On the other hand, dielectric- or semiconductor-based nanophotonic sensors can achieve a very narrow transmission line width (<1 nm), which gives a larger intensity change, but their sensitivity and dynamic range are lower compared to their plasmonic counterparts. Therefore, there is a trade-off in selecting the material platform for nanophotonic structures for integration with CMOS detectors for sensing applications, and it depends mainly on the intended applications. In the present work, we selected periodic metallic nanostructures to integrate with CMOS PDs owing to their higher sensitivity, larger dynamic range, and ease of fabrication. Different metallic nanostructure designs have been used in the past by several groups to demonstrate refractive index sensing.^{28–34} These designs include arrays of nanodiscs,²⁸ arrays of nanoholes,^{29–31} nanoslits,^{32–34} and concentric circles.³⁵ Furthermore, different metals that support the surface plasmon modes were used such as gold,^{28–33} silver,^{26,34,36} and aluminum.^{37,38}

We used a periodic array of gold nanodiscs to act as a plasmonic sensor in our sensor system. A commercial finite element method (FEM)-based simulation software, Comsol Multiphysics, was used to design an array of gold nanodiscs whose physical parameters (thickness, diameter of nanodiscs, and array period) were optimized to have the resonance wavelength close to a region where sensitivity of the PD is high (600 nm in our CMOS PD, not shown here). The design was further optimized to achieve the best possible trade-off between narrow line width and large spectral contrast. The numerically estimated optimum physical parameters of the gold nanodisc arrays are thickness, $t = 60$ nm, diameter, $d = 200$ nm, and periodicity, $a = 450$ nm. Such a structure has a resonance dip at 750 nm and a full width at half-maximum (fwhm) of 80 nm, and spectral contrast of 60%, respectively, as shown in Figure 1a. Due to the low plasma frequency of gold, it is difficult to design gold nanodisc arrays with a resonance wavelength below 700 nm without compromising on the spectral contrast. Therefore, the most optimum design has a resonance wavelength that is higher than the most sensitive wavelength range of the PD but is still within a range where responsivity of the PD is reasonably high.

Despite this small drawback of using gold, we consider it to be superior to using other metals. Aluminum can be used to cover the whole visible range,^{38,39} but it is not biocompatible. Silver is another alternative, but both aluminum and silver suffer from high oxidation rate, a problem that can be solved by using a thin passivation layer but at the cost of reduced sensitivity because the maximum electric field strength in the nanodisc structure is confined to the metal–dielectric interface and decreases exponentially away from it, as shown in Figure 2a and b. The field profile in the yz plane (cross section) is presented in Figure 2c, which shows a silica spacer layer isolating the field around the nanodiscs from the passivation layer of the CMOS chip.

Fabrication. Gold nanodiscs were first fabricated on a glass substrate as test samples to optimize the performance of the structures and measure their sensitivity. The samples were fabricated by e-beam lithography followed by a lift-off process. A 200 nm PMMA bilayer was used as the e-beam resist. The nanodiscs were defined in the resist by e-beam exposure

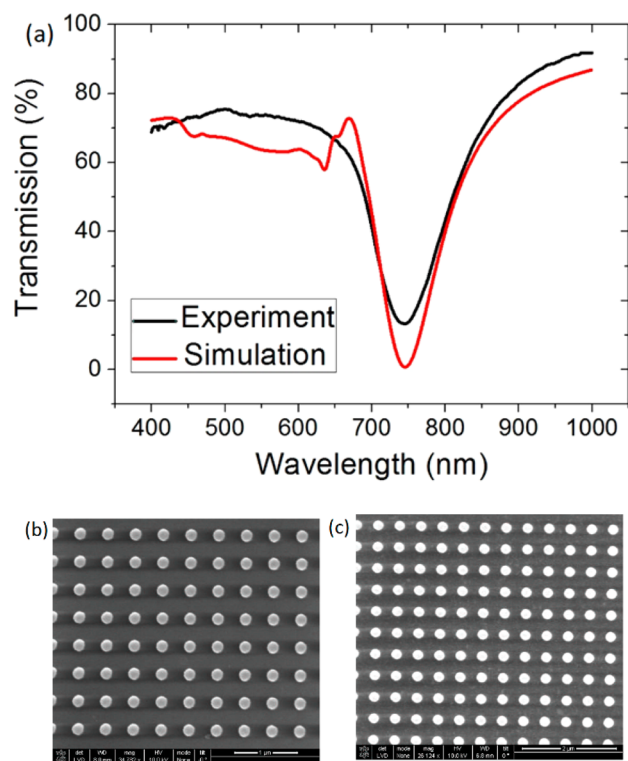


Figure 1. (a) Simulated (red) and measured (black) transmission spectrum of a gold nanodisc array on a glass slide. (b) SEM image of gold nanodiscs on a glass slide. (c) SEM image of gold nanodiscs fabricated on top of a CMOS chip.

followed by development in 2:1 IPA/MIBK developer. Next 60 nm of gold was evaporated followed by a lift-off process using acetone to remove the resist underneath the unwanted metal areas. To promote better adhesion of gold to the glass substrate, a 3 nm titanium layer was deposited prior to gold deposition. The influence of this thin titanium layer on the optical properties is not significant when the thickness of gold is kept constant.⁴⁰ A scanning electron microscope (SEM) image of the nanodisc array fabricated on the glass substrate is shown in Figure 1b.

Characterization. The transmission measurements were carried out using a commercial microspectrometer (Foster and Freeman) with a resolution of 1 nm. Unpolarized light from a halogen lamp was used as the incident light source. The light transmitted through the sample was collected by a 4× objective having a numerical aperture of 0.1 and guided to the spectrometer via an optical fiber. The measured transmission spectrum of the gold nanodisc array with the physical parameters stated in the design section is shown in Figure 1a (black curve). The experimental transmission curve (black) is compared with the simulation (red) and shows a perfect match in terms of resonance wavelength and fwhm. However, there is a slight mismatch in spectral contrast between the experimental and simulated transmission spectrum. The small peak appearing at 675 nm in the simulated spectrum corresponds to the spectral position of Rayleigh–Wood anomaly, which can be calculated analytically by using the following equation.⁴¹

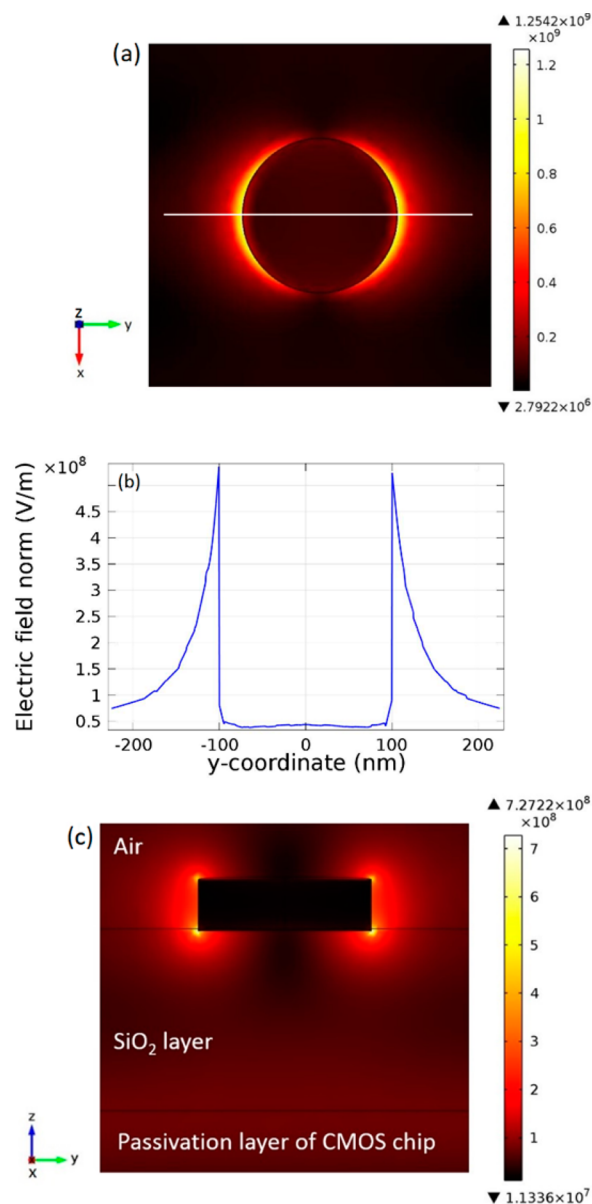


Figure 2. (a) Electric field profile at the plasmon resonance. The incident field is polarized in the y -direction. (b) Decay of the electric field as a function of distance from the metal–dielectric interface. (c) Mode profile in the yz plane showing that a silica spacer layer (300 nm in this simulation) is enough to separate the field profile of the nanodiscs from the passivation layer of the CMOS chip.

$$\left(\frac{n_2}{\lambda_0}\right)^2 - \left(\frac{n_1}{\lambda_0}\right)^2 \sin^2 \theta - 2 \frac{n_1}{\lambda_0} \sin \theta \left(\frac{n}{p} \cos \phi + \frac{m}{p} \sin \phi\right) = \frac{n^2 + m^2}{p^2} \quad (1)$$

where λ_0 is the Rayleigh–Wood anomaly wavelength, n_1 and n_2 are refractive indices of cladding and substrate, respectively, θ is the angle of incidence, ϕ is the azimuthal angle between plane of incidence and the xz plane, and n , m correspond to integer values of the diffraction order. For normal incidence ($\theta = 0$), air cladding ($n_1 = 1.0$), glass substrate ($n_2 = 1.5$), and $(n, m) = (1, 0)$ the analytically calculated wavelength of the Rayleigh–Wood

anomaly is 675 nm, which matches well with the numerically calculated value.

Sensitivity Analysis. The sensitivity of the gold nanodisc arrays to the bulk change in the refractive index of the surrounding environment was measured by applying different concentrations of glycerol on top of the nanodiscs. Increasing the concentration of glycerol increases the refractive index ($\Delta n \approx 0.01$ for 10% change in concentration)⁴² and causes a red shift of the resonance wavelength. The refractive index values for different weight/weight concentration (w/w %) of glycerol in DI water is taken from ref 42. The change in resonance wavelength for increasing concentrations of glycerol shows a linear trend, as presented in Figure 3, which corresponds to an

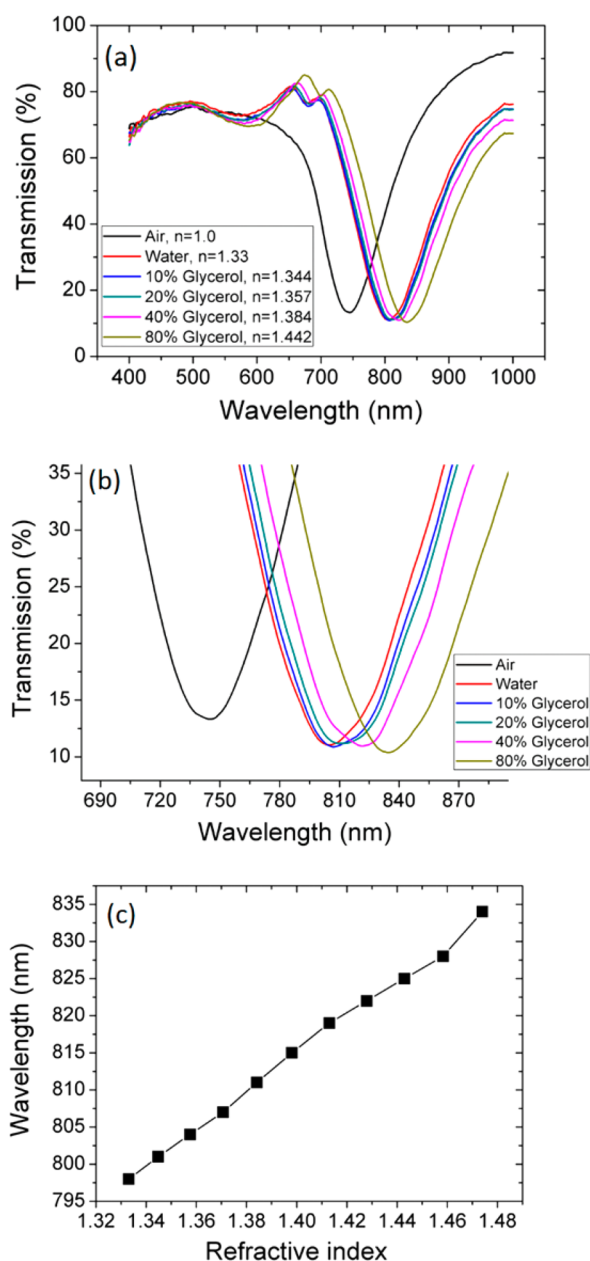


Figure 3. (a) Resonance wavelength shift due to change in refractive index corresponding to different concentrations (w/w %) of glycerol. (b) Zoomed-in view of (a). (c) Values of resonance wavelength for different refractive indices corresponding to different concentrations of glycerol.

almost linear change in the refractive index for different concentrations of glycerol. Only selected curves are shown for the purpose of clarity. From Figure 3c, the sensitivity ($\Delta\lambda/\Delta n$) of the device is determined to be 275 nm/RIU.

■ INTEGRATION OF GOLD NANODISC ARRAYS WITH CMOS DETECTOR

CMOS Detector. A CMOS integrated circuit with a photodiode was fabricated in a commercial foundry (Austria microsystems, Austria) using a 0.35 μm , four metal high voltage CMOS process. The PD has dimensions of only $6 \times 8 \mu\text{m}$. Figure 4a shows the location, encircled with a black circle, of

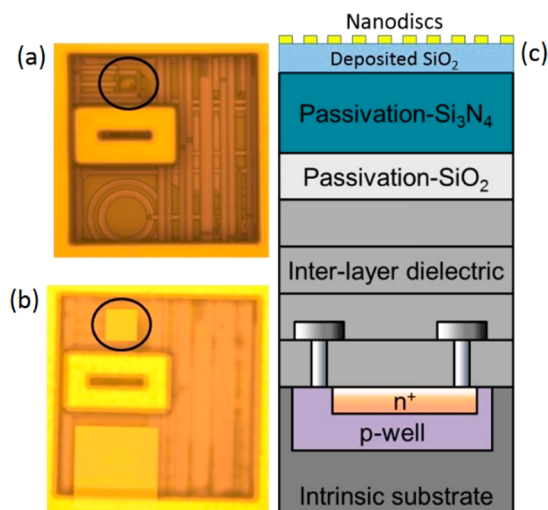


Figure 4. Microscopic image (100 \times) showing (a) the PD in the CMOS chip and (b) a gold nanodisc array fabricated on top of a PD (circled in black). (c) Cross-section schematic of the CMOS chip with deposited silica layer and gold nanodiscs fabricated on top.

the PD in the CMOS chip, while Figure 4b shows an optical image of the gold nanodiscs fabricated on top of the PD. The cross section of the CMOS chip through the PD is shown in Figure 4c.

Integration. The top passivation layer of the CMOS chips manufactured by the AMS foundry is made of silicon nitride or silicon oxy-nitride, as shown in Figure 4c, which has a higher refractive index (≈ 2.0) compared to silica (≈ 1.5) at 750 nm. Fabricating gold nanodiscs with the same dimensions as the test samples directly on top of the passivation layer will shift the resonance to longer wavelengths, where the sensitivity of the CMOS PD is lower. As shown in Figure 2c, a silica spacer layer can be deposited on top of a CMOS chip to isolate the interaction of the field around the nanodiscs from the silicon nitride passivation layer. Although simulations show that a 300 nm silica layer is enough to isolate the nanodiscs from the passivation layer, to be fully sure we deposited a 500 nm thick silica layer to keep the resonance wavelength of the nanodiscs within the high sensitivity range of the CMOS PD. Depositing a silica layer also reduces the unevenness in the surface profile of the CMOS chip, which reduces the challenge associated with fabricating nanostructures on top of the CMOS chip due to its uneven surface. The gold nanodiscs were then fabricated on top of the deposited silica layer by e-beam lithography following the same fabrication procedure as for the gold nanodiscs fabricated on glass substrates. The nanodiscs were aligned on top of the PDs by using the alignment markers defined in the CMOS

chip. An optical microscope image showing an array of gold nanodiscs on top of a PD sensor in the CMOS chip is shown in Figure 4b.

A SEM image of the gold nanodiscs fabricated on top of the CMOS chip is shown in Figure 1c. Comparing Figure 1b and c shows that the quality of the nanodiscs fabricated on top of the CMOS chip is as good as those fabricated on top of the glass substrate.

To measure the resonance response of the nanodiscs integrated with the CMOS chip, instead of transmission, a reflection measurement was carried out using a commercial microspectrometer (Foster and Freeman), as it is not possible to measure the transmission response of this integrated system. The reflection spectrum of the gold nanodiscs integrated with the CMOS chip and having an air surrounding is shown in Figure 5. The reflection spectrum of the gold nanodiscs was

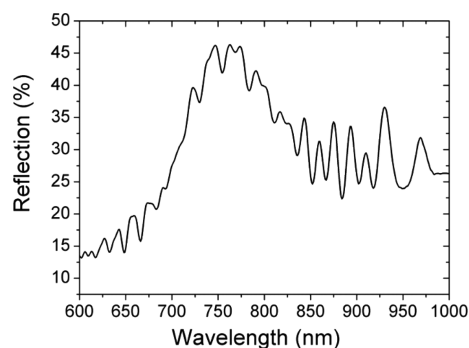


Figure 5. Optical reflection spectrum of nanodisc arrays monolithically integrated with a CMOS PD and having air as a surrounding.

normalized to a gold mirror. The reflection curve is noisy due to back reflection from different layers of the CMOS chip, which not only gives rise to Fabry–Perot fringes, similar to the ones shown in an earlier report,⁴³ but also broadens the line width. The response can be improved by etching away the passivation layer, but doing so roughens the surface, making fabrication of nanostructures on top of it challenging. In spite of these imposed Fabry–Perot fringes, the reflection curve still gives a good picture of the resonance wavelength of the CMOS-integrated gold nanodiscs, which is comparable to the resonance wavelength measured in the test samples.

After fabrication of the gold nanodisc arrays on top of the CMOS chip, the chip was mounted onto a PGA-120 chip carrier (Spectrum Semiconductor Materials, USA). It was then wire bonded and encapsulated with EPO-TEK 302-3M epoxy (Epoxy Technology, USA) to provide electrical connections and protection for subsequent aqueous experiments. To operate the PD CMOS chip, an instrumentation system was constructed to obtain the voltage signal from the PD. It consists of a laptop, an ARM mbed Integrated Development Environment STM32 Nucleo-F334R8 board (STMicroelectronics, UK), a custom-printed circuit board (Newbury Electronics, UK), and a package chip.

The chip was powered by a power supply at 3.3 V. The whole operation of the system was controlled by the software package LabVIEW (National Instruments, UK), which was programmed to read the real-time voltage signal from the PD in a synchronous manner. An encapsulated ring was attached around the chip to contain the liquid analyte for carrying out experiments with aqueous solutions. The packaged device with readout circuitry is shown in Figure 6.



Figure 6. Packaged CMOS-integrated plasmonic sensor chip with direct electrical readout.

RESULTS AND DISCUSSION

Electrical responses of the PD with monolithically integrated gold nanodiscs and the PD without disks were acquired by scanning the wavelength of incident light. To scan the whole visible range, we used a monochromator with a halogen lamp as an input light source. A comparison of the PD electrical response with and without monolithically integrated gold nanodiscs is given in Figure 7.

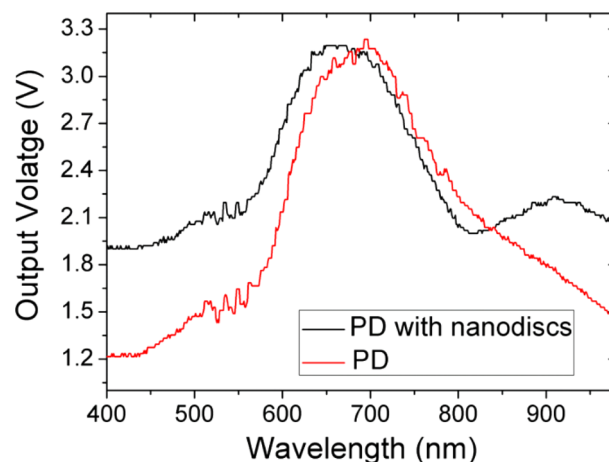


Figure 7. Comparison of electrical spectra of gold nanodiscs integrated with PD (black curve) with bare PD (red curve). The valley centered at 815 nm of the black curve corresponds to the resonance dip of the gold nanodiscs.

It has been observed that the PDs with integrated gold nanodiscs have a higher dark current compared to PDs without the discs. The postprocessing of CMOS chips to integrate nanodiscs involves high energy e-beam exposure and plasma etching. Both processes can create defect centers in the PD area and are most likely to be responsible for increasing the dark current. A dip in the output voltage of the PD integrated with gold nanodiscs can be observed around 780–825 nm, which corresponds to the transmission dip/reflection peak of the gold nanodiscs caused by the plasmon resonance. The minimum voltage point is at 815 nm. Note that the electrical response shown in Figure 7 is the convoluted response of the monochromator and detector, which is the reason for observing

the minimum voltage point at a wavelength higher than the resonance wavelength of the gold nanodiscs.

For sensitivity measurements, the wavelength of incident light was fixed at 815 nm. We used a monochromator as the incident light source; however in principle a cheap light-emitting diode (LED) could be used as the source. Keeping the input wavelength fixed at 815 nm, the electrical response of the PD was recorded for different refractive indices of the environment surrounding the gold nanodiscs. For the applied bias voltage, the current flowing through the chip is only 10 mA, which does not cause any significant thermal effects that could potentially influence the measurements. Similar to section 2, water was first added to induce a large change in the refractive index (1.0 to 1.33), and then the refractive index was changed systematically in smaller steps by applying different concentrations of glycerol ($\Delta n = 0.01$ approximately for 10% change in concentration).⁴² The change in transmitted light intensity due to a red shift of the resonance wavelength of the gold nanodisc structures for increasing concentrations of glycerol was measured directly as a change in the output voltage of the PD. The change in voltage is linear, as shown in Figure 8,

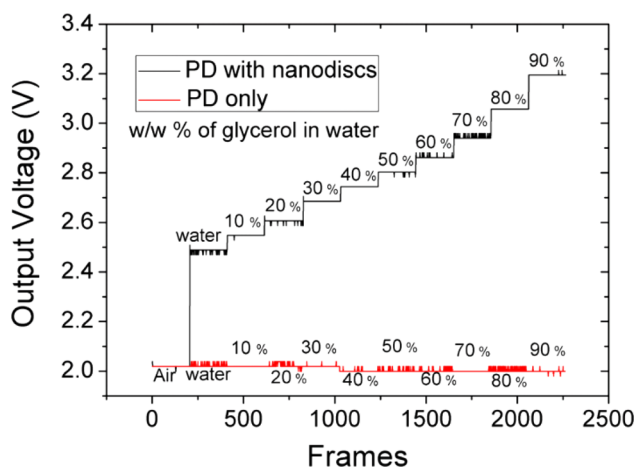


Figure 8. Electrical readout of a CMOS-integrated plasmonic sensor at $\lambda = 815$ nm. The change in intensity due to a red shift of the resonance wavelength of the nanodiscs for increasing concentrations of glycerol is measured as an increase in the output voltage of the PD.

and is consistent with the corresponding optical response of the gold nanodiscs shown in Figure 3c. Our sensor system is able to measure a minimum 10% change in glycerol concentration, which corresponds to a refractive index change of approximately 0.011.⁴² Hence, the smallest detectable refractive index change by the integrated device is 0.011.

The sensitivity of the device is measured to be 5.8 V/RIU for different concentrations of glycerol. On the other hand there is no change in the output voltage of the PD without gold nanodiscs when the refractive index is changed by adding water and different concentrations of glycerol as shown in Figure 8 (red curve). The comparison of the output voltages of the PDs with and without integrated gold nanodiscs when the refractive index is changed shows that the increase in the output voltage of the PD with integrated nanodiscs is due to the change in intensity by the resonance wavelength shift of the nanodiscs. This also eliminates the possibility of contribution of any other effects such as absorption or signal drift.

As a proof-of-principle demonstration of the device for biosensing applications, we determined the sensing response

when a layer of protein A is deposited on top of gold nanodiscs. Protein A was diluted in a PBS buffer to create a 100 $\mu\text{g}/\text{mL}$ protein A solution. The solution was applied on top of the gold nanodiscs and left for 1 h to ensure proper adsorption of protein A on the gold nanodiscs' surface. The sample was then rinsed with a PBS solution followed by DI water and dried using a nitrogen gun. An identical experiment was run in parallel on the witness sample (gold nanodiscs on a glass substrate) to determine the degree of wavelength shift caused by protein A adsorption. From the test experiment it is found that the adsorption of 100 $\mu\text{g}/\text{mL}$ protein A causes a 6 nm red shift of the resonance wavelength, as shown Figure 9a. The

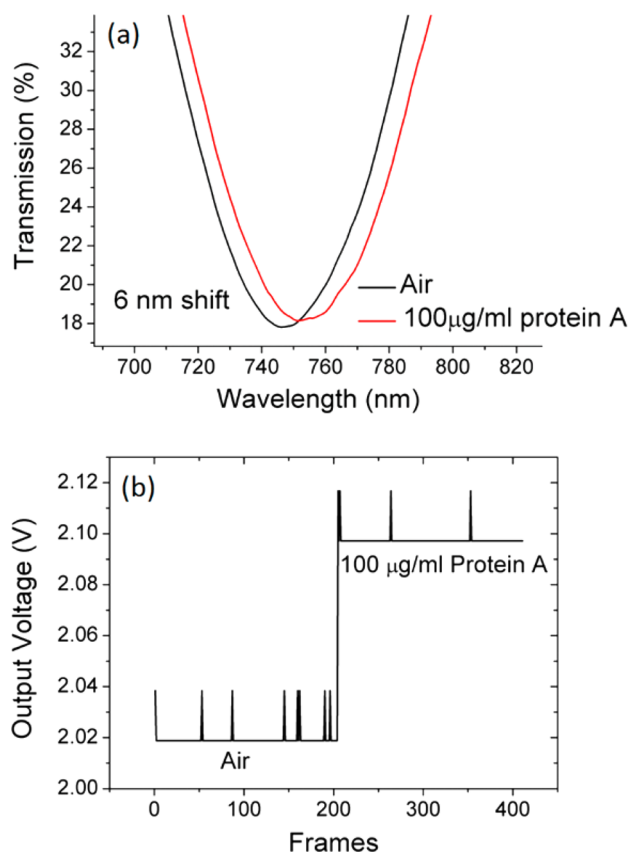


Figure 9. (a) Resonance wavelength shift due to change in refractive index by protein A adsorption on gold nanodiscs. (b) Change in output voltage of the PD due to a red shift of the resonance wavelength of the nanodiscs by protein adsorption at $\lambda = 815$ nm.

localized change in the refractive index due to protein A adsorption on gold nanodiscs integrated monolithically with the CMOS chip is detected by an increase in the output voltage of the PD as shown in Figure 9b.

The voltage change measured by the sensor when 100 $\mu\text{g}/\text{mL}$ protein A is applied is 0.08 V, which is close to the minimum voltage change measured in glycerol experiments (0.06 V for 10% change in glycerol concentration, shown in Figure 8). As shown in Figure 3, a 10% change in glycerol concentration gives a 2 nm wavelength shift. Hence, we believe that the actual wavelength shift when 100 $\mu\text{g}/\text{mL}$ protein A is applied to nanodiscs integrated with the CMOS chip is around 2–3 nm even though in glass slide samples the measured shift is 6 nm. This difference arises due to the variation between the surface profiles of glass substrate and the CMOS chip. The surface profile affects the way protein is bound to nanodiscs and

the corresponding wavelength shift. Please note that the spikes in the graph are related to the electronic data acquisition.

While this experiment shows the working of the device for detecting a nonspecifically bound protein layer, the future work will pursue sensing specific binding of the target molecules by improving the performance of the device.

CONCLUSIONS

By successfully integrating plasmonic nanostructures (an array of gold nanodiscs) with a CMOS photodiode to have a direct electrical readout system, we have demonstrated a packaged and miniaturized nanophotonic sensor system. This monolithic electronic–photonic convergence has removed the so-called “chip in a lab” bottleneck in the widespread applicability of nanophotonic sensor chips by removing the requirement of using external bulky and costly equipment for their readout. While the present work is based on a single PD, it can be further extended by making an array of PDs in a CMOS chip, which will open the door to run multiple sensing measurements on the same chip simultaneously by incorporating multiplexing technologies such as microfluidic channels.

AUTHOR INFORMATION

Corresponding Authors

*E-mail: abdul.shakoor@glasgow.ac.uk.

*E-mail: david.cumming.2@glasgow.ac.uk.

Notes

The authors declare no competing financial interest.

ACKNOWLEDGMENTS

We acknowledge the technical staff of James Watt Nanofabrication Center (JWNC) for assisting in the fabrication of samples. This work was supported by the Engineering and Physical Sciences Research Council (EPSRC) grant EP/K021966/1. The data set for this work can be accessed by following DOI: 10.5525/gla.researchdata.295.

REFERENCES

- (1) Iniewski, K. *CMOS Biomicrosystems*; Iniewski, K., Ed.; John Wiley & Sons, Inc.: Hoboken, NJ, USA, 2011.
- (2) Ahmed, M. U.; Saaem, I.; Wu, P. C.; Brown, A. S. Personalized Diagnostics and Biosensors: A Review of the Biology and Technology Needed for Personalized Medicine. *Crit. Rev. Biotechnol.* **2014**, *34*, 180–196.
- (3) Guo, L.; Jackman, J. A.; Yang, H. H.; Chen, P.; Cho, N. J.; Kim, D. H. Strategies for Enhancing the Sensitivity of Plasmonic Nanosensors. *Nano Today* **2015**, *10*, 213–239.
- (4) Shi, Y.; Ma, K.; Dai, D. Sensitivity Enhancement in Si Nanophotonic Waveguides Used for Refractive Index Sensing. *Sensors* **2016**, *16*, 324.
- (5) Fedyanin, D. Y.; Stebunov, Y. V. All-Nanophotonic NEMS Biosensor on a Chip. *Sci. Rep.* **2015**, *5*, 10968.
- (6) Valsecchi, C.; Brolo, A. G. Periodic Metallic Nanostructures as Plasmonic Chemical Sensors. *Langmuir* **2013**, *29*, 5638–5649.
- (7) Anker, J. N.; Hall, W. P.; Lyandres, O.; Shah, N. C.; Zhao, J.; Van Duyne, R. P. Biosensing with Plasmonic Nanosensors. *Nat. Mater.* **2008**, *7*, 442–453.
- (8) Stewart, M. E.; Anderton, C. R.; Thompson, L. B.; Maria, J.; Gray, S. K.; Rogers, J. A.; Nuzzo, R. G. Nanostructured Plasmonic Sensors. *Chem. Rev.* **2008**, *108*, 494–521.
- (9) Wang, J.; Yao, Z.; Poon, A. W. Silicon-Nitride-Based Integrated Optofluidic Biochemical Sensors Using a Coupled-Resonator Optical Waveguide. *Front. Mater.* **2015**, *2*, 1–13.

(10) Muellner, P.; Melnik, E.; Koppitsch, G.; Kraft, J.; Schrank, F.; Hainberger, R. CMOS-Compatible Si₃N₄ Waveguides for Optical Biosensing. *Procedia Eng.* **2015**, *120*, 578–581.

(11) Dorfner, D. F.; Hürlimann, T.; Zabel, T.; Frandsen, L. H.; Abstreiter, G.; Finley, J. J. Silicon Photonic Crystal Nanostructures for Refractive Index Sensing. *Appl. Phys. Lett.* **2008**, *93*, 2006–2009.

(12) Di Falco, A.; O’Faolain, L.; Krauss, T. F. Chemical Sensing in Slotted Photonic Crystal Heterostructure Cavities. *Appl. Phys. Lett.* **2009**, *94*, 249–251.

(13) Scullion, M. G.; Di Falco, A.; Krauss, T. F. Slotted Photonic Crystal Cavities with Integrated Microfluidics for Biosensing Applications. *Biosens. Bioelectron.* **2011**, *27*, 101–105.

(14) Sun, Y.; Fan, X. Optical Ring Resonators for Biochemical and Chemical Sensing. *Anal. Bioanal. Chem.* **2011**, *399*, 205–211.

(15) Vollmer, F.; Yang, L.; Fainman, S. Label-Free Detection with High-Q Microcavities: A Review of Biosensing Mechanisms for Integrated Devices. *Nanophotonics* **2012**, *1*, 267–291.

(16) Barrios, C. A. Optical Slot-Waveguide Based Biochemical Sensors. *Sensors* **2009**, *9*, 4751–4765.

(17) Mukundan, H.; Anderson, A. S.; Grace, W. K.; Grace, K. M.; Hartman, N.; Martinez, J. S.; Swanson, B. I. Waveguide-Based Biosensors for Pathogen Detection. *Sensors* **2009**, *9*, 5783–5809.

(18) Dell’Olio, F.; Passaro, V. M. Optical Sensing by Optimized Silicon Slot Waveguides. *Opt. Express* **2007**, *15*, 4977.

(19) Schmid, J. H.; Sinclair, W.; García, J.; Janz, S.; Lapointe, J.; Poitras, D.; Li, Y.; Mischki, T.; Lopinski, G.; Cheben, P.; et al. Silicon-on-Insulator Guided Mode Resonant Grating for Evanescent Field Molecular Sensing. *Opt. Express* **2009**, *17*, 18371.

(20) Sun, T.; Kan, S.; Marriott, G.; Chang-Hasnain, C. High-Contrast Grating Resonators for Label-Free Detection of Disease Biomarkers. *Sci. Rep.* **2016**, *6*, 27482.

(21) Hong, L.; Mcmanus, S.; Yang, H.; Sengupta, K. A Fully Integrated CMOS Fluorescence Biosensor with on-Chip Nanophotonic Filter. *Symposium on VLSI circuits* **2015**, 206–207.

(22) Cetin, A. E.; Coskun, A. F.; Galarreta, B. C.; Huang, M.; Herman, D.; Ozcan, A.; Altug, H. Handheld High-Throughput Plasmonic Biosensor Using Computational on-Chip Imaging. *Light: Sci. Appl.* **2014**, *3*, e122.

(23) Mazzotta, F.; Wang, G.; Hägglund, C.; Höök, F.; Jonsson, M. P. Nanoplasmonic Biosensing with on-Chip Electrical Detection. *Biosens. Bioelectron.* **2010**, *26*, 1131–1136.

(24) White, I. M.; Fan, X. On the Performance Quantification of Resonant Refractive Index Sensors. *Opt. Express* **2008**, *16*, 1020.

(25) Gartia, M. R.; Hsiao, A.; Pokhriyal, A.; Seo, S.; Kulsharova, G.; Cunningham, B. T.; Bond, T. C.; Liu, G. L. Colorimetric Plasmon Resonance Imaging Using Nano Lycopodium Cup Arrays. *Adv. Opt. Mater.* **2013**, *1*, 68–76.

(26) Hicks, E. M.; Zhang, X.; Zou, S.; Lyandres, O.; Spears, K. G.; Schatz, G. C.; Van Duyne, R. P. Plasmonic Properties of Film over Nanowell Surfaces Fabricated by Nanosphere Lithography. *J. Phys. Chem. B* **2005**, *109*, 22351–22358.

(27) McPhillips, J.; Murphy, A.; Jonsson, M. P.; Hendren, W. R.; Atkinson, R.; Höök, F.; Zayats, A. V.; Pollard, R. J. High-Performance Biosensing Using Arrays of Plasmonic Nanotubes. *ACS Nano* **2010**, *4*, 2210–2216.

(28) Ruemmele, J. A.; Hall, W. P.; Ruvuna, L. K.; Duyne, R. P.; Van, A. Localized Surface Plasmon Resonance Imaging Instrument for Multiplexed Biosensing. *Anal. Chem.* **2013**, *85*, 4560–4566. DOI: 10.1021/ac400192f.

(29) Brolo, A. G.; Gordon, R.; Leathem, B.; Kavanagh, K. L. Surface Plasmon Sensor Based on the Enhanced Light Transmission through Arrays of Nanoholes in Gold Films. *Langmuir* **2004**, *20*, 4813–4815.

(30) De Leebeek, A.; Kumar, L. K. S.; de Lange, V.; Sinton, D.; Gordon, R.; Brolo, A. G. On-Chip Surface-Based Detection with Nanohole Arrays. *Anal. Chem.* **2007**, *79*, 4094–4100.

(31) Im, H.; Lindquist, N. C.; Lesuffleur, A.; Oh, S. H. Atomic Layer Deposition of Dielectric Overlayers for Enhancing the Optical Properties and Chemical Stability of Plasmonic Nanoholes. *ACS Nano* **2010**, *4*, 947–954.

(32) Perino, M.; Pasqualotto, E.; De Toni, A.; Garoli, D.; Scaramuzza, M.; Zilio, P.; Ongarello, T.; Paccagnella, A. Development of a Complete Plasmonic Grating-Based Sensor and Its Application for Self-Assembled Monolayer Detection. *Appl. Opt.* **2014**, *53*, 5969–5976.

(33) Lee, M. H.; Gao, H.; Odom, T. W. Refractive Index Sensing Using Quasi One-Dimensional Nanoslit Arrays. *Nano Lett.* **2009**, *9*, 2584–2588.

(34) Karabchevsky, A.; Krasnykov, O.; Auslender, M.; Hadad, B.; Goldner, A.; Abdulhalim, I. Theoretical and Experimental Investigation of Enhanced Transmission through Periodic Metal Nanoslits for Sensing in Water Environment. *Plasmonics* **2009**, *4*, 281–292.

(35) Lee, K. L.; Wang, W. S.; Wei, P. K. Comparisons of Surface Plasmon Sensitivities in Periodic Gold Nanostructures. *Plasmonics* **2008**, *3*, 119–125.

(36) Haes, a. J.; Van Duyne, R. P. A Nanoscale Optical Biosensor: Sensitivity and Selectivity of an Approach Based on the Localized Surface Plasmon Resonance Spectroscopy of Triangular Silver Nanoparticles. *J. Am. Chem. Soc.* **2002**, *124*, 10596–10604.

(37) King, N. S.; Liu, L.; Yang, X.; Cerjan, B.; Everitt, H. O.; Nordlander, P.; Halas, N. J. Fano Resonant Aluminum Nanoclusters for Plasmonic Colorimetric Sensing. *ACS Nano* **2015**, *9*, 10628–10636.

(38) Langhammer, C.; Schwind, M.; Kasemo, B.; Zoric, I. Localized Surface Plasmon Resonances in Aluminum Nanodisks. *Nano Lett.* **2008**, *8*, 1461–1471.

(39) Chen, Q.; Cumming, D. R. S. High Transmission and Low Color Cross-Talk Plasmonic Color Filters Using Triangular-Lattice Hole Arrays in Aluminum Films. *Opt. Express* **2010**, *18*, 14056.

(40) Lahiri, B.; Dylewicz, R.; De La Rue, R. M.; Johnson, N. P. Impact of Titanium Adhesion Layers on the Response of Arrays of Metallic Split-Ring Resonators (SRRs). *Opt. Express* **2010**, *18*, 11202–11208.

(41) Johansen, B.; Uhrenfeldt, C.; Larsen, A. N.; Pedersen, T. G.; Ulriksen, H. U.; Kristensen, P. K.; Jung, J.; Søndergaard, T.; Pedersen, K. Optical Transmission through Two-Dimensional Arrays of β -Sn Nanoparticles. *Phys. Rev. B: Condens. Matter Mater. Phys.* **2011**, *84*, 113405.

(42) Hoyt, L. F. New Table of the Refractive Index of Pure Glycerol at 20°C. *Ind. Eng. Chem.* **1934**, *26*, 329–332.

(43) Chen, Q.; Chitnis, D.; Walls, K.; Drysdale, T. D.; Collins, S.; Cumming, D. R. S. CMOS Photodetectors Integrated With Plasmonic Color Filters. *IEEE Photonics Technol. Lett.* **2012**, *24*, 197–199.